高等学校化学学报
CHEMICAL JOURNAL OF CHINESE UNIVERSITIES
研究论文

表面羧基构型与润湿性之间的热力学关联

郭卓欢，汪大洋
（吉林大学化学学院，无机合成与制备化学国家重点实验室，长春 130012）

摘要 以聚丙烯酸（PAA）薄膜为模型体系，通过调控分子量与固化温度，制备了一系列具有不同水润 湿性的PAA薄膜. 借助衰减全反射傅里叶变换红外光谱（ATR-FTIR）解析，将薄膜表面羧基（COOH）的分子 构型[自由羧基（$COOH_f$）和氢键结合羧基（$COOH_{HB}$）]与表面能的极性分量（$\gamma^{s,p}$）直接关联. 通过将$\gamma^{s,p}$分解为$COOH_f$和$COOH_{HB}$的贡献之和，首次获得$COOH_{HB}$的本征表面能极性分量$\gamma_{HB}^{s,p*}$为8.34 mN/m，显著低于$COOH_f$的$\gamma_f^{s,p*}$（34 mN/m），这一结果表明氢键作用显著降低了表面的$\gamma^{s,p}$，合理解释了PAA薄膜表面较大水接触角的差异，并为通过润湿性反推表面$COOH_{HB}$的比例提供了热力学基础. 进一步将该模型推广至羧基自组装单层（COOH-SAMs）体系时发现，表面COOH密度（∑COOH）对润湿行为具有关键调控作用：当∑COOH处于4.30~5.25 nm^{-2}时，COOH以自由态为主并可形成有效水合层，最有利于超亲水表面的实现. 本研究不仅建立了表面COOH构型与宏观润湿性之间的定量热力学模型，还通过推广至COOH-SAMs体系验证了该模型的普适性，为多种COOH功能化表面亲水性的可控设计提供了统一理论框架.

关键词 聚丙烯酸薄膜；氢键；衰减全反射傅里叶变换红外光谱；羧基构型定量；表面能极性分量
中图分类号 O647 **文献标志码** A doi：10.7503/cjcu20250303

Thermodynamic Correlation Between Surface Carboxyl Configuration and Wettability

GUO Zhuohuan, WANG Dayang*
(*State Key Laboratory of Inorganic Synthesis and Preparative Chemistry*, *College of Chemistry*, *Jilin University*, *Changchun* 130012, *China*)

Abstract In this study, polyacrylic acid (PAA) films were employed as a model system, and a series of PAA films with tunable water wettability was systematically prepared by varying molecular weight and curing temperature. Using attenuated total reflectance Fourier-transform infrared spectroscopy (ATR-FTIR), the molecular configurations of surface carboxyl groups (COOH), free carboxyl ($COOH_f$) and hydrogen-bonded carboxyl ($COOH_{HB}$), were directly correlated with the polar component of surface energy ($\gamma^{s,p}$). By decomposing the $\gamma^{s,p}$ values of the PAA thin films as a sum of the contributions of $COOH_f$ and $COOH_{HB}$, the intrinsic polar component of surface energy of $COOH_{HB}$ ($\gamma_{HB}^{s,p*}$) was quantified for the first time as 8.34 mN/m, significantly lower than that of $COOH_f$ ($\gamma_f^{s,p*}$=34 mN/m). This result highlights that hydrogen bonding markedly reduces the $\gamma^{s,p}$, providing a rational explanation for the relatively large water contact angle observed on PAA thin films. Furthermore, it establishes a thermodynamic basis for estimating the fraction of surface $COOH_{HB}$ groups (f_{HB}) from wettability measurements. Further extension of the model to carboxyl-terminated self-assembled monolayers (COOH-SAMs) revealed that surface COOH density (∑COOH) critically regulates wetting behavior: when ∑COOH ranges from 4.30 to 5.25 nm^{-2}, COOH groups predominantly exist in a free state and facilitate effective hydration layers, thereby promoting superhydrophilicity. Overall, this study not only

收稿日期：2025-10-18. 网络首发日期：2025-11-21.
联系人简介：汪大洋，男，博士，教授，主要从事胶体界面科学基础问题方面的研究. E-mail：wangdayang@jlu.edu.cn
基金项目：国家自然科学基金（批准号：21932003）资助.
Supported by the National Natural Science Foundation of China(No.21932003).

establishes a unified thermodynamic framework linking surface COOH configurations to macroscopic wettability, but also validates its universality by extending it to COOH-SAMs systems, thereby providing a unified theoretical framework for the controllable design of hydrophilicity in various COOH-functionalized surfaces.

Keywords Polyacrylic acid film; Hydrogen bonding; Attenuated total reflectance Fourier-transform infrared spectroscopy; Quantitative carboxyl configuration; Polar component of surface energy

1 Introduction

Polar carboxyl groups (COOH) are widely utilized in functional films, surface modifications, self-assembled monolayers (SAMs) and biointerfaces due to their excellent hydrophilicity and biocompatibility[1—5]. However, even surfaces nominally rich in COOH groups exhibit substantial variation in water wettability: reported water contact angles on COOH-functionalized surfaces range from 0° to 50°[6—11], indicating that high COOH groups content does not necessarily guarantee superhydrophilicity. This behavior primarily arises from two factors: hydrogen bonding among surface COOH groups and the formation of hydrogen-bonded networks involving interfacial water molecules (COOH···H_2O···COOH). Both effects reduce the contribution of COOH groups to surface wettability, leading to a decrease in the polar component of surface energy ($\gamma^{s,p}$). While molecular dynamics and quantum chemical simulations have revealed local mechanisms[12—16], a unified method to quantitatively distinguish between free ($COOH_f$) and hydrogen-bonded ($COOH_{HB}$) carboxyl configurations and directly correlate them to macroscopic wettability remains lacking.

In this study, polyacrylic acid (PAA) thin films were used as a model system, with surface wettability systematically tuned *via* molecular weight and curing temperature. Combining contact angle measurements and ATR-FTIR spectroscopy, we established an experimental framework linking the fractions of $COOH_f$ and $COOH_{HB}$ (f_f and f_{HB}) to macroscopic water wettability ($\theta_{w/a}$) through the polar component $\gamma^{s,p}$. By deconvoluting of the O—H stretching band in ATR-FTIR spectra, we decomposed the $\gamma^{s,p}$ of the PAA thin films into the intrinsic contributions of surface $COOH_f$ and $COOH_{HB}$ groups, γ_f^{s,p^*} and γ_{HB}^{s,p^*}, as described in Equation (1):

$$\gamma^{s,p} = f_f\gamma_f^{s,p^*} + f_{HB}\gamma_{HB}^{s,p^*} \quad (1)$$

For the first time, γ_{HB}^{s,p^*} was determined as 8.34 mN/m, significantly lower than γ_f^{s,p^*} (34 mN/m)[17], rationalizing the relatively large water contact angle observed on PAA surfaces ($\theta_{w/a}$ of approx. 77°). Using γ_{HB}^{s,p^*} and Equation (1), the surface fractions f_f and f_{HB} can be quantitatively predicted from $\theta_{w/a}$ values.

Based on the above framework, the model was further applied to COOH-SAMs to investigate their anomalous wettability[18]. The role of ∑COOH in regulating surface wettability was systematically analyzed, and the configurational distribution of surface COOH groups across different ∑COOH ranges was clarified. It was found that when ∑COOH is in the range of 4.30—5.25 nm^{-2}, surface COOH groups predominantly exist in the free state and can form an effective hydration layer, favoring the emergence of superhydrophilicity. Overall, this study establishes, for the first time, a quantitative thermodynamic model that correlates the surface configuration of COOH with macroscopic wettability, overcoming the limitations of previous studies that only qualitatively discussed hydrogen-bonding effects[11,18]. The successful extension of this model to COOH-SAMs underscores its broad applicability across diverse COOH-functionalized materials, providing a unified theoretical basis for interpreting anomalous wetting behavior and facilitating the rational design of surfaces with tailored hydrophilicity.

2 Experimental

2.1 Materials and Apparatuses

Polyacrylic acid (M_w *ca.* 1250000) (H_PAA), polyacrylic acid (M_w *ca.* 450000) (M_PAA) and polyacrylic

acid solution(M_w *ca.* 100000)(L_PAA), purity≥99.9%, Sigma-Aldrich Co., Ltd., Shanghai.

MFP-3D Bio atomic force microscope(AFM), Asylum Research, USA; DSA100 Contact angle goniometer, KRÜSS GmbH, Germany; Nicolet Aratar 370 Attenuated total reflection Fourier transform infrared spectrometer(ATR-FTIR), Thermo Scientific, USA.

2.2 Methods

2.2.1 Preparation of PAA solutions Aqueous H_PAA and M_PAA solutions were prepared by dissolving predetermined amounts of PAA powder in deionized water at 100 ℃ under magnetic stirring(900 r/min) for more than 2 h. After complete dissolution, the solutions were cooled to room temperature, filtered to remove insoluble impurities, and adjusted to a final concentration of 1%(mass fraction). Similarly, the L_PAA solution was prepared by dissolving a 35%(mass fraction) PAA stock solution in deionized water at 25 ℃ under magnetic stirring(900 r/min). After complete dissolution, the solution was adjusted to a final concentration of 1%(mass fraction).

2.2.2 Preparation of PAA thin films Aliquots(200 μL) of the prepared aqueous H_PAA, M_PAA and L_PAA solutions were drop-cast onto glass slides(2.5 cm×2.5 cm) to form thin films, followed by drying for 1 h at 20, 60, 100, 140 or 170 ℃, respectively. Subsequently, the films were dried for 24 h at room temperature in a desiccator. The drying time of 1 h was intentionally chosen to minimize the risk of heating-induced surface reconstruction, particularly at higher temperatures. The resulting model films were denoted as H_PAA^T, M_PAA^T and L_PAA^T, where the superscript "T" indicates the temperature of the initial drying stage.

2.2.3 ATR-FTIR Characterization ATR-FTIR was carried out on a Nicolet Aratar 370 attenuated total reflection Fourier transform spectrometer, in which zinc selenide crystals were used as internal reflecting elements at an incidence angle of 45° with a penetration depth of approximately 0.5—1.0 μm(based on ZnSe crystal calculations), ensuring surface sensitivity.

2.2.4 Surface wettability analysis Contact angle measurements were performed using a drop shape analyser at ambient temperature. Prior to testing, the as-prepared PAA thin films were stored in a desiccator at 25 ℃ and 25%—30% relative humidity for 24 h to ensure measurement consistency. The static water contact angle ($\theta_{w/a}$) was determined by depositing a 2 μL water droplet on the film surface. For each sample, the $\theta_{w/a}$ value was reported as the average of three measurements collected at different positions on the surface after equilibration of the droplet for 10 s.

The total surface free energy (γ^s), as well as its polar interaction component ($\gamma^{s,p}$) and dispersive component ($\gamma^{s,d}$) components, were calculated based on Fowkes's model for a water-air system[19], according to Equations (2) and (3):

$$\gamma_w(1+\cos\theta_{w/a}) = 2\sqrt{\gamma^{s,d}\gamma_w^d} + 2\sqrt{\gamma^{s,p}\gamma_w^p} \tag{2}$$

$$\sqrt{\gamma_o^d}\,(1+\cos\theta_{o/a}) = 2\sqrt{\gamma^{s,d}} \tag{3}$$

where γ_w is 72.8 mN/m, γ_w^d is 21.8 mN/m and γ_w^p is 51.0 mN/m.

2.2.5 Calculation of the packing density of COOH groups The packing density of COOH groups per unit area($\sum$COOH, nm^{-2}) was calculated as:

$$\sum \mathrm{COOH} = \sum \mathrm{PAA} N_s \tag{4}$$

where $\sum$COOH represents the packing density of PAA molecular chains per unit area, and N_s is the number of repeating units within the corresponding occupied area. The value of $\sum$COOH was determined according to:

$$\sum \mathrm{PAA} = \frac{cV_m N_A}{M} \tag{5}$$

where c is the mass concentration of the PAA solution, V_m is the volume of PAA solution within a unit area (1 nm^2), based on the film preparation process described in Section 2.2.2(drop-casting 200 μL of solution

onto a substrate with an area of 6.25 cm^2), V_m is calculated to be 32 μL, M is the molecular weight of PAA, and N_A is the Avogadro's constant. The surface area occupied by a single PAA molecular chain can then be expressed as:

$$A_{PAA} = 1/\sum PAA \quad (6)$$

Correspondingly, the Flory radius is given by:

$$R_F = \mathcal{L}_K N_s^{0.6} \approx \left(\frac{A_{PAA}}{\pi}\right)^{0.5} \quad (7)$$

where $\mathcal{L}_K$ denotes the Kuhn length(0.154 nm). Based on Equation (4), the packing density of COOH groups per unit area can thus be obtained[20~22].

3 Results and Discussion

3.1 Water Wettability of PAA Thin Films

Uniform and water-insoluble PAA thin films can be easily obtained by drop-casting aqueous PAA solutions onto hydrophilic substrates, which facilitates stable characterization. A key feature of these films is the strong tendency of COOH side groups in PAA chains to form extensive hydrogen-bonding networks. As reported in previous studies[23], the rotational radius (R_F) of PAA chains in aqueous solutions of equal concentration depends on both the molecular weight of PAA and the temperature, thereby enabling adjustment of the fraction of $COOH_{HB}$ in the resulting thin films. To investigate the influence of hydrogen bonding among surface COOH groups on the water wettability of PAA thin films, PAA samples with high, medium and low molecular weights (H_PAA, M_PAA and L_PAA) were selected. As described in Section 2.2.2, aqueous solutions of these polymers were cast into thin films and subsequently cured at 20, 60, 100, 140 or 170 ℃, generating a series of model surfaces (H_PAA^T, M_PAA^T and L_PAA^T). As shown in AFM images [Fig.1(A)—(C)], H_PAA^T thin films exhibited excellent smoothness, with RMS roughness values ranging from 4.734 to 4.795 nm across different curing temperatures. This indicates that although high-temperature treatment may induce local chain rearrangement, it does not significantly alter the surface flatness, thereby ruling out a dominant influence of surface microstructures on the wetting behavior. The thickness of all prepared PAA thin films, confirmed by profilometer measurements, was uniform and approximately in the range of 6—7 μm. This thickness range ensures that the subsequent ATR-FTIR analysis and contact angle measurements primarily reflect surface properties rather than bulk phase effects. Fig.1(D) demonstrates that the $\theta_{w/a}$ of H_PAA^T and M_PAA^T thin films decreased markedly with increasing curing temperature from 20 to 140 ℃ (H_PAA^T: from 77.7° to 52.5°; M_PAA^T: from 68.5° to 48.7°), suggesting enhanced hydrophilicity. The moderate hydrophilicity indicates that surface COOH groups preferentially formed inter-chain hydrogen bonds rather than hydrogen bonding with water molecules. These inter-chain hydrogen bonds were disrupted upon curing, particularly at 100—140 ℃, consistent with the glass transition temperature of PAA (95—105 ℃), where increased chain mobility facilitates bond breakage. Literature has further indicated that curing at 140 ℃ most effectively disrupts hydrogen bonds[24]. In contrast, the wettability of L_PAA^T thin films remained nearly unchanged, with $\theta_{w/a}$ values maintained between 27°—30°, reflecting negligible hydrogen-bond interactions. At 170 ℃, the $\theta_{w/a}$ of all thin films increased significantly, attributed to partial dehydration of COOH groups into anhydrides, which are less hydrophilic than carboxyl groups[25]. As shown in Fig.1(E), the unexpectedly low $\gamma^{s,p}$ of H_PAA^T and M_PAA^T thin films confirmed the strong negative effect of inter-chain hydrogen bonding. Specifically, $\gamma^{s,p}$ values of H_PAA$^{20\,℃}$ 和 M_PAA$^{20\,℃}$ were only 7.7 and 9.2 mN/m, respectively, far below the theoretical maximum ($\gamma_f^{s,p*}$ of 34.0 mN/m) expected from free COOH groups. Upon increasing the curing temperature to 140 ℃, disruption of $COOH_{HB}$ groups released $COOH_f$, leading to ~3 times and ~2 times

increases in $\gamma^{s,p}$ for H_PAA^{T} and M_PAA^{T} thin films, respectively. By contrast, both the $\gamma^{s,p}$ and $\theta_{w/a}$ of L_PAA^{T} thin films remained stable, consistent with their negligible hydrogen-bonding capacity.

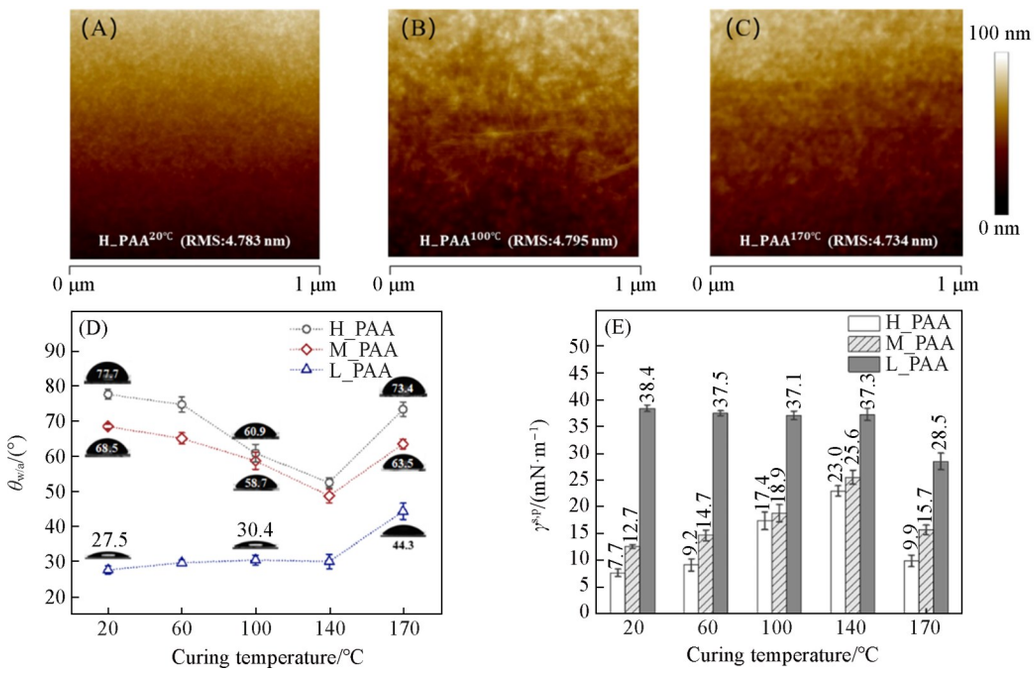


Fig. 1 AFM images of as-prepared H_PAA$^{20\,℃}$ thin film(A), H_PAA$^{100\,℃}$ thin film(B) and H_PAA$^{170\,℃}$ thin film(C) with the corresponding RMS values marked, plot of the $\theta_{w/a}$ values of as-prepared H_PAA^{T}, M_PAA^{T} and L_PAA^{T} thin films *versus* the curing temperature(T), in which the photos of a 2 μL droplet of water placed on the corresponding thin films are shown(D) and histograms of the values of $\gamma^{s,p}$ of as-prepared H_PAA^{T}, M_PAA^{T} and L_PAA^{T} thin films(E)

3.2 ATR-FTIR Characterization of Hydrogen Bonding in PAA Thin Films

To further elucidate the variation in hydrogen bonding among surface COOH groups of PAA thin films with curing temperature, ATR-FTIR spectra of H_PAA^{T}, M_PAA^{T} and L_PAA^{T} thin films were collected. PAA exhibits broad COOH-associated absorption bands due to hydrogen-bonded structures[26~28]. All spectra were background-subtracted and normalized to ensure consistency, and the main band assignments are summarized in Table 1. At a curing temperature of 170 ℃, a distinct absorption band appeared at 1526 cm^{-1} for all three types of PAA films[Fig.2(A)—(C)]. This band was attributed to the formation of anhydrides *via* dehydration of COOH groups[25], which accounts for the increase in $\theta_{w/a}$ and the reduction in $\gamma^{s,p}$ observed above 140 ℃ [Fig.1(D) and (E)]. In the range of 20—140 ℃, two broad O—H stretching bands were observed in the 3600—3000 cm^{-1} region. The lower-frequency band was assigned to the stretching vibration of $COOH_{HB}$,

Table 1 Infrared bands of PAA thin films

Wavenumber/cm^{-1}	Assignment
3600—3000(broad)	O—H stretching
2930	CH_2 stretching
2500—2700(broad)	Overtones and combinations of bands near 1412 and 1238 cm^{-1} enhanced by Fermi resonance
1695—1725(strong)	C=O stretching
1526	Acid anhydride stretching
1457	CH_2 deformation
1412, 1238, 1165	C—O stretching coupled with O—H in-plane bending
846	C—COOH stretching

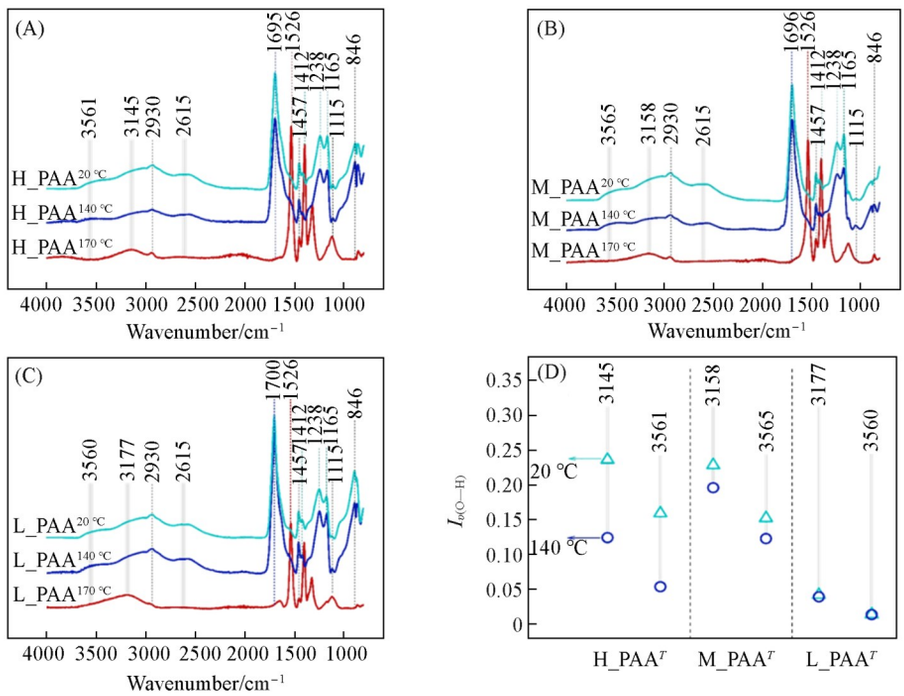


Fig. 2 ATR-FTIR spectra of H_PAA^T(A), M_PAA^T(B) and L_PAA^T(C) thin films in the range of 4000—400 cm^{-1} and the summary of the O—H stretching vibration peak intensity on the surface of H_PAA^T, M_PAA^T and L_PAA^T thin films(D)

while the higher-frequency band was attributed to hydrogen bonding between COOH groups and H_2O molecules[29]. With decreasing molecular weight, the maximum of the low-frequency O—H band shifted progressively from 3145 cm^{-1}(H_PAA^T) to 3158 cm^{-1}(M_PAA^T) and finally to 3177 cm^{-1}(L_PAA^T). Since the position of O—H stretching bands reflects the distribution of hydrogen-bonding strength, this shift indicates that the average hydrogen-bonding strength on the surface of L_PAA^T thin films was significantly lower than that of H_PAA^T and M_PAA^T thin films, consistent with the lower $\theta_{w/a}$ values of L_PAA^T. As shown in Fig.2(D), the absolute absorbance of the O—H stretching bands (normalized to the C—H band at 2930 cm^{-1}) also reflected the variation in hydrogen bonding. As curing temperature increased from 20 ℃ to 140 ℃, the O—H band absorbance of H_PAA^T and M_PAA^T thin films decreased significantly, whereas that of L_PAA^T thin films remained nearly unchanged. These results confirm that increasing temperature disrupts inter-chain hydrogen bonding in H_PAA^T and M_PAA^T thin films, accompanied by the release of $COOH_f$ and an increase in surface hydrophilicity. In addition, a sharp band was observed at 1695—1700 cm^{-1}, which was attributed to intermolecular hydrogen bonding between polymer carbonyl groups[30]. The position and absorbance of this band in the three types of PAA films exhibited similar trends to those of the O—H stretching bands, further confirming the influence of curing temperature and molecular weight on hydrogen-bonding interactions. Other characteristic absorption bands appeared at 2615, 1457, 1412, 1238, 1165 and 846 cm^{-1}. Specifically, the band at 2615 cm^{-1} corresponded to overtones and combination bands near 1412 and 1238 cm^{-1} were enhanced by Fermi resonance; the band at 1457 cm^{-1} was assigned to CH_2 deformation; the bands at 1412, 1238 and 1165 cm^{-1} were attributed to C—O stretching coupled with O—H in-plane bending; and the band at 846 cm^{-1} was assigned to C—COOH stretching. These assignments are consistent with previous reports[31,32].

3.3 Quantitative Expression of the Contributions of Hydrogen-bonded COOH Groups to the Surface Energy Polar Components of PAA Thin Films

Based on the well-established use of ATR-FTIR peak areas for quantifying surface chemical

compositions, deconvolution of the O—H stretching bands was employed to estimate the fractions of $COOH_f$ and $COOH_{HB}$ in PAA thin films. These fractions are denoted as $f_f^{M,T}$ and $f_{HB}^{M,T}$, where "M" specifies the molecular weight of PAA and "T" specities the curing temperature. Their quantitative relationship with the water wettability of PAA films was subsequently analyzed. The relevant equations are given as follows:

$$A_i^{M,T} = dc_i^{M,T}\int_0^{+\infty}\varepsilon_i(v)d_v \tag{8}$$

$$f_{HB}^{M,T} = c_{HB}^{M,T}/c_{COOH}^{M,T} = A_{HB}^{M,T}/A_{COOH}^{M,T} \tag{9}$$

$$f_f^{M,T} + f_{HB}^{M,T} = 1 \tag{10}$$

Here, $A_i^{M,T}$ represents the integrated intensity of the vibrational bands of $COOH_f$ or $COOH_{HB}$, $c_i^{M,T}$ is their concentration (per unit volume or surface area), d is the detection pathway length, and $\varepsilon_i(v)$ is the wavenumber-dependent absorption coefficient. In Equation (9), $A_{HB}^{M,T}$ is the integrated intensity of the $COOH_{HB}$ bands and $c_{HB}^{M,T}$ is their concentration, while $A_{COOH}^{M,T}$ and $c_{COOH}^{M,T}$ represents the total COOH bands.

Because the vibrational band of $COOH_f$ is barely visible in the ATR-FTIR spectra of PAA thin films [Fig.3(A)], direct estimation of $A_{COOH}^{M,T}$ (or $c_{COOH}^{M,T}$) was not feasible. To overcome this limitation, values of $f_f^{M,T}$ and $f_{HB}^{M,T}$ were estimated following a literature-reported calibration[17]. Specifically, for COOH-terminated self-assembled monolayers (COOH-SAMs), where surface COOH groups are fully exposed and inter-group hydrogen bonding is negligible, f_{HB}^{SAMs} can be reasonably assumed to be 0.01. Accordingly, $f_{HB}^{M,T}$ of PAA thin films was estimated using:

$$f_{HB}^{M,T} = f_{HB}^{SAMs}(A_{HB}^{M,T}/A_{HB}^{SAMs}) \tag{11}$$

The derived $f_f^{M,T}$ and $f_{HB}^{M,T}$ values, summarized in Table 2, were obtained from the integrated intensities of $COOH_{HB}$ bands. As shown in Fig.3(B), increasing PAA thin films surface hydrophilicity was accompanied by a significant rise in $f_f^{M,T}$ and a corresponding decline in $f_{HB}^{M,T}$, providing quantitative evidence for the temperature-induced disruption of $COOH_{HB}$ groups.

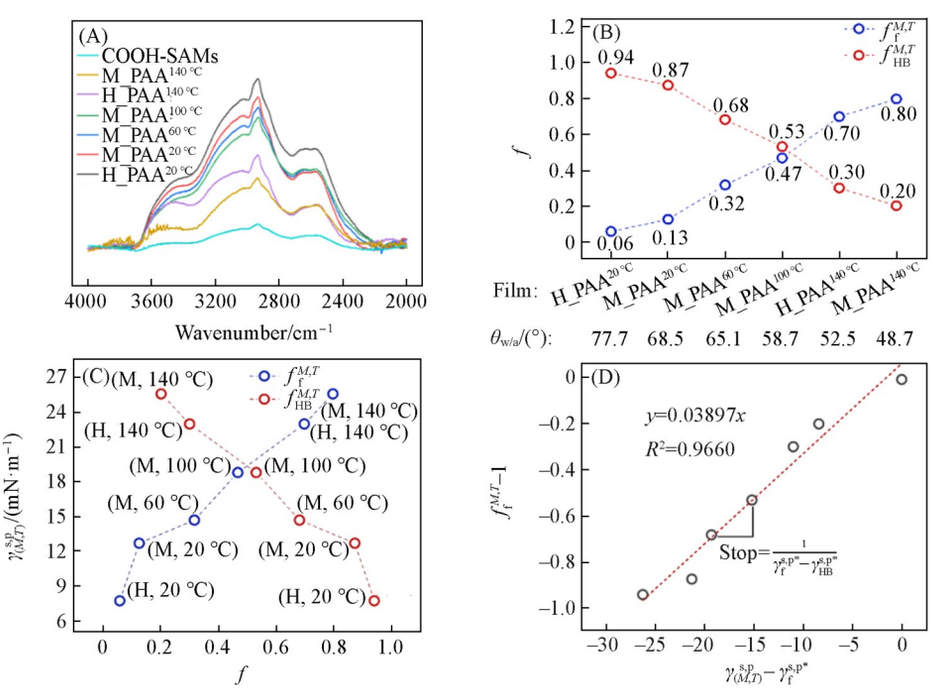


Fig. 3 ATR-FTIR spectra of COOH-SAMs and PAA thin films in the range of 4000—2000 cm^{-1}(A), plots of the calculated $f_f^{M,T}$ and $f_{HB}^{M,T}$ values of as-prepared PAA thin films *versus* the $\theta_{w/a}$(B), plots of the $\gamma_{(M,T)}^{s,p}$ values of as-prepared PAA thin films *versus* their $f_f^{M,T}$ and $f_{HB}^{M,T}$ values(C), and plots of the $f_f^{M,T}$−1 values of as-prepared COOH-SAMs and PAA thin films *versus* their $\gamma_{(M,T)}^{s,p} - \gamma_f^{s,p*}$ values(D)

Table 2 Summary of the values of $A_{HB}^{M,T}$, $f_{HB}^{M,T}$, $f_f^{M,T}$ and $\gamma_{(M,T)}^{s,p}$ of as-prepared COOH-SAMs and PAA thin films

COOH Surface	COOH-SAMs	H_PAA$^{20\,℃}$	M_PAA$^{20\,℃}$	M_PAA$^{60\,℃}$	M_PAA$^{100\,℃}$	H_PAA$^{140\,℃}$	M_PAA$^{140\,℃}$
$A_{HB}^{M,T}$	2.02	190.10	176.40	137.80	107.40	60.87	40.89
$f_{HB}^{M,T}$	0.0100	0.9410	0.8736	0.6822	0.5317	0.3013	0.2024
$f_f^{M,T}$	0.9900	0.0590	0.1264	0.3178	0.4683	0.6987	0.7976
$\gamma_{(M,T)}^{s,p}$	34.00	7.72	12.70	14.70	18.80	23.00	25.60

The polar component of surface free energy $\gamma^{s,p}$, denoted as $\gamma_{(M,T)}^{s,p}$[Fig.1(E)], was then plotted against $f_f^{M,T}$ and $f_{HB}^{M,T}$. The results clearly indicate that the increase in $\gamma^{s,p}$ arises from the conversion of $COOH_{HB}$ into $COOH_f$ groups with increasing curing temperature[Fig.3(C)]. Assuming that surface $COOH_f$ and $COOH_{HB}$ contribute independently to $\gamma^{s,p}$——γ_f^{s,p^*} and γ_{HB}^{s,p^*}, the following relation can be established:

$$\gamma_{(M,T)}^{s,p} = f_f^{M,T}\gamma_f^{s,p^*} + f_{HB}^{M,T}\gamma_{HB}^{s,p^*} \tag{12}$$

which can be rearranged as:

$$f_f^{M,T} - 1 = \frac{1}{\left(\gamma_f^{s,p^*} - \gamma_{HB}^{s,p^*}\right)}\left(\gamma_{(M,T)}^{s,p} - \gamma_f^{s,p^*}\right) \tag{13}$$

By fitting Equation (13) to the experimental data in Table 2 using a linear regression model[Fig.3(D)], the intrinsic polar contribution of hydrogen-bonded COOH groups was determined as γ_{HB}^{s,p^*}=8.34 mN/m. Consequently, the $\gamma^{s,p}$ of as-prepared PAA thin films can be expressed as the weighted sum of contributions from surface $COOH_f$ and $COOH_{HB}$ groups ($\gamma_f^{s,p}$ and $\gamma_{HB}^{s,p}$) according to Equation (1). Notably, γ_{HB}^{s,p^*} (8.34 mN/m) is significantly lower than γ_f^{s,p^*} (34 mN/m), and its corresponding polar energy contribution is approximately 1.05 kJ/mol, which is substantially less than the 4.28 kJ/mol for $COOH_f$ groups. This result quantitatively demonstrates, from an energetic perspective, the "passivation" effect of hydrogen bonding on the surface activity of carboxyl groups. It provides a rational explanation for the differences in $\theta_{w/a}$ observed on PAA thin films and deepens the understanding of the mechanism by which hydrogen bonding regulates surface wettability.

3.4 Extension of γ_{HB}^{s,p^*} to COOH-SAMs Wettability

The γ_{HB}^{s,p^*} value obtained in Section 3.3 represents the intrinsic contribution of $COOH_{HB}$ to the $\gamma^{s,p}$ in PAA thin films. This intrinsic value is expected to be generally applicable to all COOH-containing surfaces, irrespective of preparation methods. On this basis, γ_{HB}^{s,p^*} can be employed to quantitatively analyze wettability anomalies frequently observed on COOH-functionalized surfaces. A representative case is the study by Fang *et al.*[18], who investigated the wettability of COOH-terminated self-assembled monolayers (COOH-SAMs) by combining molecular dynamics simulations and quantum chemical calculations. They reported that at a surface COOH packing density ($\sum$COOH) of 3.71—4.30 nm^{-2}, water molecules ($\sum H_2O$=2.0 nm^{-2}) could be embedded between adjacent COOH groups to form COOH···H_2O···COOH hydrogen-bonded complexes. These internal hydrogen-bonding networks reduce the accessibility of COOH groups for hydrogen bonding with interfacial water, resulting in water contact angles greater than 34°, in contrast to θ=0° when $\sum$COOH exceeds 4.30 nm^{-2}. Hence, assuming that the wettability of COOH-SAMs surfaces with $\sum$COOH between 3.71—4.30 nm^{-2} is entirely attributed to COOH···H_2O···COOH hydrogen-bonded complexes, their contribution to surface wettability can be expressed as:

$$\gamma_{HB}^{s,p} = f_t\gamma_{HB}^{s,p^*} \tag{14}$$

When $\sum$COOH>4.30 nm^{-2}, all surface COOH groups exist as $COOH_f$, and $\gamma_f^{s,p}$ is given by:

$$\gamma_f^{s,p} = f_t\gamma_f^{s,p^*} \tag{15}$$

where f_t = 1, the contribution of nonpolar regions to $\gamma_{HB}^{s,p}$ and $\gamma_f^{s,p}$ were neglected, since their intrinsic value (≈2.2 mN/m) is negligible. As shown in Fig.4(A), the θ_{HB}^{cal} and θ_f^{cal} values, calculated from $\gamma_{HB}^{s,p}$ and $\gamma_f^{s,p}$ using

Equation (2), were 76.4° and 35.7°, respectively. These values show a significant deviation of nearly 30° from the reported experimental values, although θ_f^{cal} aligns with the θ value for COOH-SAMs with ∑COOH of 3.71—4.30 nm^{-2} in the literature. This discrepancy, however, contradicts the assumption that the surface wettability is governed by the COOH···H_2O···COOH hydrogen-bonded complexes.

Considering that for ∑COOH=3.71—5.05 nm^{-2}, the mean inter-COOH group distance (s=0.30—0.21 nm) is relatively large, the COOH groups are loosely packed. This s can be calculated using the following combined equations:

$$\sum \mathrm{COOH} \cdot \frac{4}{3}\pi \cdot \frac{l}{2} \cdot \frac{l}{2} \cdot \frac{d_1}{2} = 1\mathrm{nm}^2 \cdot d_1 \cdot 0.74 \tag{16}$$

$$l = \sqrt{\frac{6 \times 0.74}{\pi \sum \mathrm{COOH}}} \tag{17}$$

$$s = l - d_1 \tag{18}$$

In Equation (16), it is assumed that the COOH groups adopt a hexagonal close-packed arrangement [Fig.4(B)]. Here, 0.74 represents the maximum packing efficiency of hard spheres in three-dimensional close packing. The variable l refers to the nearest-neighbor separation distance, and d_1 is the molecular diameter of the COOH groups (d_1=0.318 nm)[33]. This allows for the formation of hydration layers by adsorbing water molecules during air-water contact. Therefore, the intrinsic polar contribution of $COOH_f$ should be corrected to account for hydration effects, expressed as:

$$\gamma_{f,hydra}^{s,p^*} = \frac{\gamma_f^{s,p^*} + 3\gamma_w^p}{4} \tag{19}$$

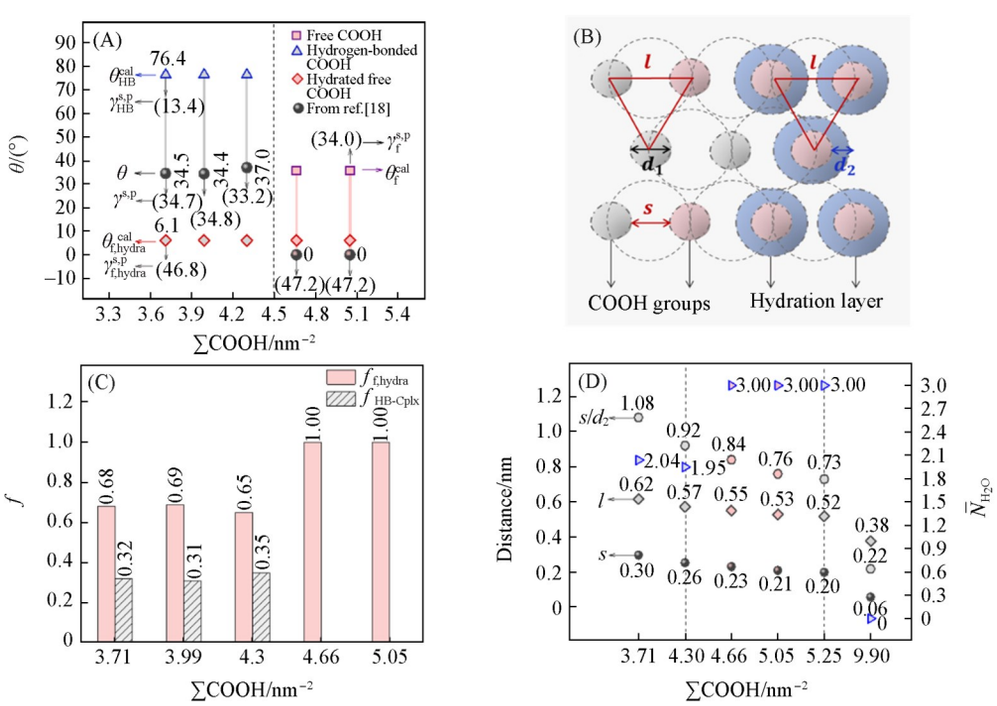


Fig. 4 Summary of the literature-reported water contact angles(θ) and corresponding polar components of surface free energy($\gamma^{s,p}$) for COOH-SAMs surfaces at different ∑COOH values, together with theoretical $\gamma^{s,p}$ values calculated without hydration($\gamma_{HB}^{s,p}$ and $\gamma_f^{s,p}$) and with hydration ($\gamma_{f,hydra}^{s,p}$), as well as the corresponding theoretical contact angles θ_{HB}^{cal}, θ_f^{cal} and $\theta_{f,hydra}^{cal}$(A), schematic illustration of the monolayer structure of COOH groups organized in a hexagonal arrangement(B), histogram of $f_{f,hydra}$ and $f_{HB\text{-}Cplx}$ values for COOH-SAMs surfaces at different ∑COOH values(C) and summary of l, s, s/d_2 and $\bar{N}_{H_2O}$ for COOH-SAMs surfaces at different ∑COOH values(D)

Here, it is assumed that each $COOH_f$ group adsorbs up to 3 water molecules[34], and $\gamma^{s,p^*}_{f,hydra}$ represents the weighted mean of γ^{s,p^*}_f and γ^p_w. Substituting $\gamma^{s,p^*}_{f,hydra}$ for γ^{s,p^*}_f in Equation (15) allows for the calculation of the hydration-corrected contribution $\gamma^{s,p}_{f,hydra}$. As shown in Fig.4(A), the hydration effect significantly enhances the contribution of the surface polar regions. The $\theta^{cal}_{f,hydra}$ value calculated from $\gamma^{s,p}_{f,hydra}$(6.1°) closely matches the reported experimental value of 0°, demonstrating that the hydration effect of $COOH_f$ groups on the surface wettability of COOH-SAMs is substantial and cannot be ignored. Therefore, the observed $\gamma^{s,p}$ for COOH-SAMs with ∑COOH=3.71—4.30 nm^{-2} arises from a combination of hydrated $COOH_f$ and COOH···H_2O···COOH hydrogen-bonded complexes, expressed as:

$$\gamma^{s,p} = f_{f,hydra}\gamma^{s,p^*}_{f,hydra} + f_{HB\text{-}Cplx}\gamma^{s,p^*}_{HB} \quad (20)$$

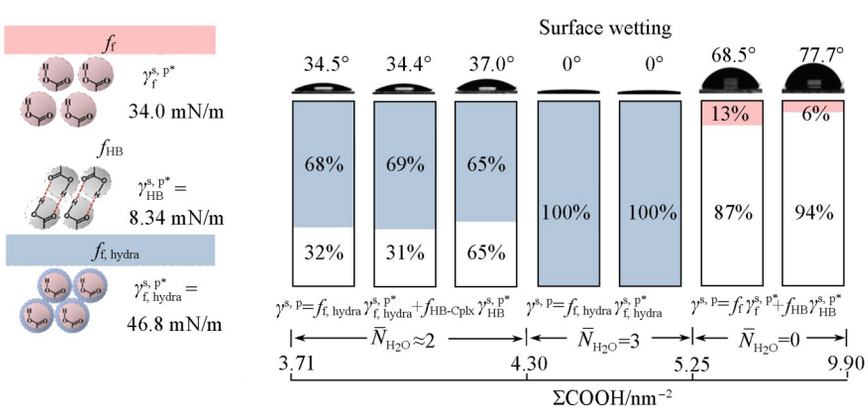
$$f_{f,hydra} + f_{HB\text{-}Cplx} = 1 \quad (21)$$

By solving Equations (20) and (21), the true fractions of $f_{f,hydra}$ and $f_{HB\text{-}Cplx}$ can be extracted[Fig.4(C)]. When the hydration effect of the water molecules adsorbed by the hydrated $COOH_f$ groups is distributed among all COOH groups using Equation (22), we find that the average number of water molecules associated with each COOH group, $\bar{N}_{H_2O}$, is approximately 2, which is in excellent agreement with the reported value of ∑H_2O=2.0 nm^{-2}.

$$\bar{N}_{H_2O} = \frac{3f_{f,hydra}\sum COOH}{\sum COOH} \quad (22)$$

It is noteworthy that at ∑COOH=3.71—4.30 nm^{-2}, the hydrogen-bonded complexes on the surface of COOH-SAMs are in a dynamic equilibrium. However, the overall presence of COOH groups on the surface at any given time consists of a combination of hydrated $COOH_f$ and COOH···H_2O···COOH hydrogen-bonded complexes. When ∑COOH>4.30 nm^{-2}, the surface consists entirely of hydrated $COOH_f$ groups, with each COOH group averaging 3 associated water molecules[Fig.4(D)]. As shown in Fig.4(D), the s/d_2 value for COOH-SAMs surfaces with ∑COOH=3.71—4.30 nm^{-2} ranges from 0.92 to 1.08(where d_2 is the diameter of a water molecule, 0.276 nm)[35]. This suggests that under these conditions, water molecules can be embedded between adjacent COOH groups to form COOH···H_2O···COOH hydrogen-bonded complexes, which diminishes the surface wettability. In contrast, for ∑COOH>4.30 nm^{-2}, water molecules adsorb on the surface to form a hydration layer, promoting surface hydrophilicity.

Finally, it is noteworthy that in our work, H_PAA^T and M_PAA^T thin films exhibited surface ∑COOH values of 9.36 and 9.89 nm^{-2}, respectively (Section 2.2.4), yet displayed unexpectedly high $\theta_{w/a}$ values (68°—77°)(Scheme 1). This behavior can be attributed to the extremely close packing of COOH groups at



Scheme 1 Schematic illustration of the composition of surface COOH groups configuration at different ∑COOH ranges, marking the corresponding values of water contact angles($\theta_{w/a}$), f_f, f_{HB}, $f_{f,hydra}$, γ^{s,p^*}_f, γ^{s,p^*}_{HB}, $\gamma^{s,p^*}_{f,hydra}$ and the average number of water molecules associated with each COOH group($\bar{N}_{H_2O}$)

such high densities, where the mean inter-COOH group distance is less than 0.2 nm (the critical distance for hydrogen bonding) [Fig. 4(D)]. Under these conditions, COOH groups preferentially form inter-group hydrogen bonds instead of hydration layers, thereby suppressing surface hydrophilicity. Consequently, when designing superhydrophilic COOH-functionalized surfaces, maintaining $\sum$COOH values in the range of 4.30—5.25 nm^{-2} is most appropriate, as this regime favors the predominance of free COOH groups and the effective formation of hydration layers.

4 Conclusions

Studies have demonstrated that the macroscopic wettability of PAA thin films is strongly influenced by the relative fractions of $COOH_f$ and $COOH_{HB}$ groups. As the curing temperature increases, intermolecular hydrogen bonds gradually break, releasing more $COOH_f$ and thereby significantly enhancing surface hydrophilicity. Using ATR-FTIR spectroscopic analysis, the polar component of surface energy ($\gamma^{s,p}$) of PAA thin films was expressed as the weighted sum of the contributions from $COOH_f$ and $COOH_{HB}$ groups (γ_f^{s,p^*} and γ_{HB}^{s,p^*}) by the corresponding f_f and f_{HB} [Equation (1)]. This enabled us to predict the surface hydrophilicity ($\theta_{w/a}$) of PAA thin films from the molecular hydrogen bonding configurations of their surface COOH groups, namely, f_f and f_{HB} components or *vice versa*. This model is only applicable to COOH-functionalized surfaces prepared at temperatures below 140 ℃. Higher temperatures may induce dehydration of carboxyl groups to form anhydride groups, thereby affecting the accuracy of the model.

The γ_{HB}^{s,p^*} was first determined to be 8.34 mN/m, significantly lower than γ_f^{s,p^*} (34.00 mN/m), which fundamentally explains the relatively large contact angles commonly observed on PAA surfaces and highlights the key role of hydrogen bonding in regulating surface wettability. The established quantitative model was further extended to the COOH-SAMs system, the model not only predicted the proportion of COOH···H_2O···COOH hydrogen-bonded complexes at $\sum$COOH of 3.71—4.30 nm^{-2}, but also systematically revealed the critical role of $\sum$COOH in regulating wettability. When $\sum$COOH is within the range of 3.71—4.30 nm^{-2}, the wettability is a combined effect of hydrated free COOH groups and hydrogen-bonded complexes. At higher $\sum$COOH (4.30—5.25 nm^{-2}), free COOH groups dominate, facilitating effective hydration and promoting superhydrophilicity. However, when $\sum$COOH exceeds 5.25 nm^{-2}, excessive carboxyl density prevents effective hydration, leading to the formation of intermolecular hydrogen bonds, which significantly suppresses surface hydrophilicity. In summary, this study provides a unified quantitative framework for understanding the "non-ideal" wettability of COOH-functionalized surfaces and establishes a theoretical basis for designing functional materials with tunable hydrophilicity and controllable interfacial energy.

References

[1] Lee H., Alcaraz M. L., Rubner M. F., Cohen R. E., *ACS Nano*, **2013**, *7*(3), 2172—2185
[2] Arima Y., Iwata H., *Biomaterials*, **2007**, *28*(20), 3074—3082
[3] Cheng Y., Feng F., Zhu T. X., Zheng Y. H., Gou Y. K., Yang D. P., Huang J. Y., Lai Y. K., Jiang Z. Y., *Chem. Eng. J.*, **2025**, *504*, 158421
[4] Rac V., Lević S., Balanč B., Graells B. O., Bijelić G., *Colloid. Surface. B*, **2019**, *180*, 441—448
[5] Xu Z., Song K., Yuan S. L., Liu C. B., *Langmuir*, **2011**, *27*(14), 8611—8620
[6] Major R. C., Houston J. E., McGrath M. J., Siepmann J. I., Zhu X. Y., *Phys. Rev. Lett.*, **2006**, *96*, 177803
[7] Tu A., Kwag H. R., Barnette A. L., Kim S. H., *Langmuir*, **2012**, *28*(43), 15263—15269
[8] Arima Y., Iwata H., *J. Mater. Chem.*, **2007**, *17*, 4079—4087
[9] Choi S., Yang Y., Chae J., *Biosens. Bioelectron.*, **2008**, *24*(4), 893—899
[10] Ohnuki H., Izumi M., Lenfant S., Guerin D., Imakubo T., Vuillaume D., *Appl. Surf. Sci.*, **2005**, *246*(4), 392—396
[11] James M., Darwish T. A., Ciampi S., Sylvester S. O., Zhang Z. M., Ng A., Gooding J. J., Hanley T. L., *Soft Matter*, **2011**, *7*, 5039

[12] Winter N., Vieceli J., Benjamin I., *J. Phys. Chem. B*, **2008**, *112*(2), 227—231
[13] Xu Z., Song K., Yuan S. L., Liu C. B., *Langmuir*, **2011**, *27*(14), 8611—8620
[14] Szori M., Jedlovszky P., Roeselova M., *Phys. Chem. Chem. Phys.*, **2010**, *12*, 4604—4616
[15] Osnis A., Sukenik C. N., Major D. T., *J. Phys. Chem. C*, **2012**, *116*(14), 770—782
[16] Stevens M. J., Grest G. S., *Biointerphases*, **2008**, *3*, FC13—FC22
[17] Ma Z. Y., Wang D. Y., *Colloid. Surface. A*, **2023**, *675*, 132031
[18] Guo P., Tu Y. S., Yang J. R., Wang C. L., Sheng N., Fang H. P., *Phys. Rev. Lett.*, **2015**, *115*, 186101
[19] Fowkes M., *J. Ind. Eng. Chem.*, **1960**, *12*, 40—52
[20] Yamakawa H., *Modern Theory of Polymer Solutions*, Harper & Row, New York, **1971**
[21] Cranford S. W., Buehler M. J., *Macromolecules*, **2012**, *45*(19), 8067—8082
[22] Han T. Y., Ma Z. Y., Wang D. Y., *ACS Macro Lett.*, **2021**, *10*, 354—358
[23] Kurapati R., Natarajan U., *Ind. Eng. Chem. Res.*, **2020**, *59*, 16099—16111
[24] Zhang W., Zhang Z. N., Wang X. P., *J. Colloid Interface Sci.*, **2009**, *333*, 346—353
[25] Maura J. J., Eustance D. J., Ratcliffe C. T., *Macromolecules*, **1987**, *20*, 196—202
[26] Bardet L., Cassanas-Fabre G., Alain M., *J. Mol. Struct.*, **1975**, *24*(1), 153—164
[27] Leyte J. C., Zuiderweg L. H., Vledder H. J., *Spectrochim. Acta*, **1967**, *23*(5), 1397—1407
[28] Lin-Vien D., Colthup N. B., Fately W. G., Grasselli J. G., *The Handbook of Infrared and Raman Characteristic Frequencies of Organic Molecules*, Academic Press, San Diego, **1991**
[29] Chen H. C., Lin H. C., Chen H. H., Mai F. D., Liu Y. C., Lin C. M., Chang C. C., Tsai H. Y., Yang C. P., *Sci. Rep.*, **2014**, *4*, 4425
[30] Kim T. H., Ahn J. H., Choi H. K., Choi Y. J., Cho C. S., *Arch. Pharm. Res.*, **2007**, *30*, 381—386
[31] Hoerter M., Oprea A., Barsan N., Weimar U., *Sens. Actuat. B*, **2008**, *134*(2), 743—749
[32] Itoh K., Yaita M., Hasegawa T., Fujii S., Misono Y., *J. Electron Spectrosc. Relat. Phenom.*, **1990**, *54/55*, 923—932
[33] Benoit R. L., Louis C., Fre'chette M., *Thermochimica Acta*, **1991**, *176*, 221—232
[34] Du D. M., Qin M., Zhou Z. Y., Fu A. P., *Int. J. Quantum Chemistry*, **2012**, *112*(2), 351—358
[35] Marcus Y., *Chem. Rev.*, **1988**, *88*, 1475—1498

(Ed.: H, K, M)